Compliant substrate epitaxy: Au on MoS_{2}

Yuzhi Zhou, Daisuke Kiriya, E. E. Haller, Joel W. Ager, III, Ali Javey, and D. C. Chrzan

Phys. Rev. B **93**, 054106 — Published 5 February 2016

DOI: 10.1103/PhysRevB.93.054106

Compliant substrate epitaxy: Au on MoS_2

Yuzhi Zhou,[1,2] Daisuke Kiriya,[3,2] E. E. Haller,[1,2] Joel W. Ager III,[1,2] Ali Javey,[3,2] and D. C. Chrzan[1,2]

[1]*Department of Materials Science and Engineering, University of California at Berkeley, Berkeley, California 94720, USA*

[2]*Materials Sciences Division, Lawrence Berkeley National Laboratory, Berkeley, California 94720, USA*

[3]*Electrical Engineering and Computer Sciences, University of California, Berkeley, California 94720, United States*

(Dated: January 12, 2016)

Abstract

A theory for the epitaxial growth of Au on MoS_2 is developed and analyzed. The theory combines continuum linear elasticity theory with density functional theory to analyze epitaxial growth in this system. It is demonstrated that if one accounts for interfacial energies and strains, the presence of misfit dislocations, and the compliance of the MoS_2 substrate, that the experimentally observed growth orientation is favored despite the fact that it represents a larger elastic mismatch than two competing structures. The stability of the experimentally preferred orientation is attributed to the formation of a large number of strong Au-S bonds, and it is noted that this strong bond may serve as a means to exfoliate and transfer large single layers sheets of MoS_2, as well as to engineer strain within single layers of MoS_2. The potential for using a van der Waals-bonded layered material as compliant substrate for applications in 2D electronic devices and epitaxial thin film growth is discussed.

I. I. INTRODUCTION

The electronic and optical properties of transition metal dichalcogenides show much promise for technological applications[1]. Incorporating this material within devices will require either the growth of the dichalcogenides on other substrates, or growth of other materials on a dichalcogenide substrate. In this respect, the growth of Au on MoS_2 can be viewed as a prototypical system.

The growth of Au on MoS_2 was studied in the mid to late 1960's using early *in situ* and *ex situ* transmission electron microscopy[2–6]. Au was deposited on MoS_2 using evaporation, and was discovered to grow predominantly with a plate-like geometry in a $\{111\}$ orientation. The $\langle 110 \rangle$ directions of the Au platelets were nearly aligned along the $\langle 11\bar{2}0 \rangle$ direction of the substrates, with a minor spread in the orientation (average rotation $\pm 0.25^\circ$). Similar orientations were observed for Ag nuclei[6]. In these experiments, the presence of misfit dislocations are also observed in the evaporated Au islands which suggests a relatively strong bonding (more than just VDW interaction) between the substrate and the film.

The growth and evolution of the Au films were modeled using theory available at the time[3,7]. This theory, however, was rooted in a phenomenological understanding of the interfacial properties. Moreover, the substrate was treated as a typical bulk, and no accounting for the influence of the van der Waals (VDW) bonding within the substrate layers was attempted. Further, the Au clusters were approximated as spherical caps, as the TEM images did not allow for measurement of island thicknesses. Finally, only the observed $\{111\}$ orientation was considered in any detail. Given the recent and growing interest in transition metal dichalcogenides for electronic and optical applications, it is timely to revisit this epitaxial growth system.

In the most simple model of epitaxy, the substrate is assumed infinite, and as a consequence, it does not relax during the growth process. For Au on MoS_2, the three possible orientations of the growing film are shown in Fig. 1. For the $\{111\}$ orientation, the biaxial strain required in the film is approximately 8%. In contrast, the strains in the $\{001\}$ oriented film are approximately -6% and 8% in the directions shown. While in the rotated $\{111\}$ orientation (that has been used to study the electronic properties of Au contacts to MoS_2 in Ref.[8]) the biaxial strain is about -6%. Based on these strains, one would expect that the $\{001\}$ orientation would be most favorable, and consequently would be predominantly

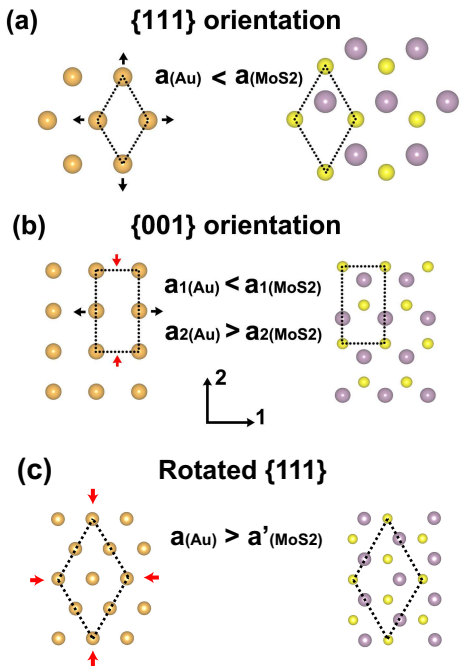

FIG. 1: (a) The strain for Au (left) and MoS_2 (right) in {111} orientation. The Molybdenum atoms are represented by purple circles, the Sulfur atoms by yellow circles and the Gold atoms by orange circles. $a_{(Au)}$ and $a_{(MoS2)}$ are the lattice constants in Au (111) plane and MoS_2 respectively. The arrows indicate the biaxial strain in this case. (b) The strain in {001} orientation. The subscripts "1" and "2" are two perpendicular directions in the plane. a_1 and a_2 are the lattice constants in corresponding directions. In this case, the sign and amount of strain in the two directions is different. (c) The strain in the rotated {111} orientation. The arrows indicate compressive biaxial strain.

the experimentally observed orientation. Figure 2 compares the elastic energies of the three films (neglecting surface and interfacial stresses and energies) as a function of the number of layers of Au grown assuming the substrate is rigid. Clearly, the elastic energy of the {111} orientation is much larger than the other two orientations. This observation raises a fundamental questions regarding the growth: Why is the predominant experimentally observed orientation {111} and not one of the other two?

In the following sections a model to explain the experimentally observed film orientation is developed. The model assumes that due to the weak VDW bonding between layers of MoS_2, the surface layer is able to relax nearly independently of the remaining bulk layers. The compliance of the substrate, when coupled with the surface and interface energies (including

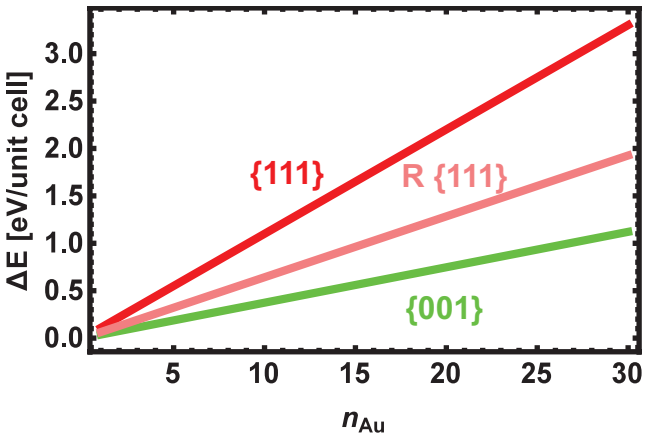

FIG. 2: The strain energy per unit cell for Au deposition on MoS_2 in three orientations computed assuming that the MoS_2 is unrelaxed, and that surface and interfacial energies make negligible contributions to the energy. The rotated {111} orientation is labeled as "R {111}".

strain energies) and misfit dislocations, results in a lower formation energy for the {111} orientation as compared to the other two orientations, in agreement with experiment. The implications of these findings are discussed.

II. II. MODEL

The model is built on two types of calculations. First, a continuum linear elastic model for the epitaxial growth of Au on MoS_2 is developed. This model includes the relaxation of the substrate and the influence of surface/interface energies but is dislocation-free. The parameters for the model are then determined using density functional theory (DFT) based electronic structure total energy methods. Finally, misfit dislocations are incorporated into our model to predict the properties of all three configurations.

A. II.1. Linear elasticity theory model

1. *II.1.1. General description*

The continuum linear elastic model is developed by proposing a "synthesis path" and then computing the energy contributions along this path. (This path is not necessarily experimentally accessible. It simply facilitates computation.) The initial step in forming an

epitaxial layer can be taken as a thin slab of the growing material being extracted from a bulk crystal. This extraction creates two surfaces, and the energy of the slab is increased by the surface energies. The next step is to strain the film to its final strain in its epitaxially bonded state. This contributes the strain energy of the bulk plus any contribution to the strain energy from the surfaces. The third step is to separate the first substrate layer from rest of the substrate to create a freestanding MoS_2 layer. This adds a layer separation energy to the system. In the fourth step, this free-standing layer is then strained introducing the strain energy of the single layer. In the fifth step, the epitaxial film is welded to the free standing layer, replacing one of the strained Au surfaces with a strained Au-MoS_2 interface. Then, the film/free-standing layer is readhered to the substrate, returning the layer separation energy to the thermal bath, but introducing the energy required to slip the top MoS_2 layer relative to the remaining layers. In addition, if misfit dislocations are introduced (after fitting the surface/interface parameters), they will relieve part of the mismatch strain in the film at the cost of misfit dislocation formation energy. Taken in total, the sum of the changes in energy for both the substrate and the epitaxial film as compared with their bulk counterparts, ΔE can be written:

$$\Delta E = E_{Au,sur} + E_{film} + E_{sub} + E_{Au/S,int} + E_{slip} + E_{dis} \tag{1}$$

where $E_{Au,sur}$ is the energy of the strained Au surface, E_{film} is the energy of the strained film neglecting surface contributions, E_{sub} is the strain energy of the first substrate layer, $E_{Au/S,int}$ is the interfacial and strain energy of the Au-MoS_2 substrate interface, and E_{slip} is the slip energy between the first layer of the substrate and the remaining substrate. E_{dis} is the formation energy of the misfit dislocation and is not included in the fitting process.

2. II.1.2. Elastic energy terms

The first four contributions to ΔE can be expressed analytically using linear elasticity theory:

$$E_{film} = \frac{1}{2} C_{f,ijkl} \epsilon_{f,ij} \epsilon_{f,kl} V_f \tag{2}$$

$$E_{sub} = \frac{1}{2} C_{sub,ijkl} \epsilon_{sub,ij} \epsilon_{sub,kl} A_{sub} \tag{3}$$

$$E_{Au,sur} = \gamma_s + f_{s,ij} \epsilon_{s,ij} + \frac{1}{2} C_{s,ijkl} \epsilon_{s,ij} \epsilon_{s,kl} A_s \tag{4}$$

$$E_{Au/S,in} = \gamma_I + f_{I,ij}\epsilon_{I,ij} + \frac{1}{2}C_{I,ijkl}\epsilon_{I,ij}\epsilon_{I,kl}A_I \quad (5)$$

The $C_{f,ijkl}$, $C_{sub,ijkl}$ are the elastic constants for the film and the top layer substrate. The strain tensors are indexed similarly. We approximate the surface/interface stress energies up to the second order of the strain tensor: γ_s and γ_I are the unstrained surface and interfacial energies, respectively; $f_{s,ij}$ and $f_{I,ij}$ are the linear surface stress terms while $C_{s,ijkl}$ and $C_{I,ijkl}$ are the quadratic terms of the surface/interface strain energies. The top layer of the substrate is treated as a 2D material. (We assume that the VDW interaction within the substrate is sufficient to insure the substrate remains flat during the epitaxial growth.) V_f is the equilibrium volume the film would have if it were part of a bulk Au crystal. A_{sub}, A_s and A_I are the reference unit cell areas for the substrate, surface and interface strains respectively. A_s and A_I are taken equal to A_f, the area covered by the Au film with its bulk lattice parameter. A_{sub} is taken to be the equilibrium area of the monolayer MoS_2 unit cell.

3. II.1.3. Slip energy estimation

The slip energy arises from displacing the top MoS_2 substrate layer relative to layers below. An approximation for this energy is made by investigating a similar slip in a bilayer MoS_2 system. In this system, two MoS_2 layers are placed relative to each other in the same way as the two adjacent layers in the bulk MoS_2. A top view of this system is in Fig. 3 with only the lattice points shown. The two layers coincide at the origin point in the top view (left corner). Each layer contains 21×21 unit cells. The Mo and S atoms are added to the lattice points in the same way as that in the two adjacent layers in the bulk MoS_2. The interlayer distance is 6.25 Å, as obtained from DFT with van der Waals corrections of the pristine bilayer MoS_2 system. To create a slip similar to the compliant substrate epitaxy system, the first layer MoS_2 is strained biaxially by 5% while the second layer is kept fixed. This is the typical amount strain in the Au-MoS_2 epitaxy system. This strain results in a structure wherein the lattice parameters of the slipped layer and the unslipped layer are commensurate (the lattice points coincide in xy plane at the corners of the strained layer). When the strain is applied, the Mo and S atoms are also displaced with the lattice points and no internal relaxation of the unit cell is allowed.

We follows Grimme's D2 method[9] to include the VDW interaction energy and calculate

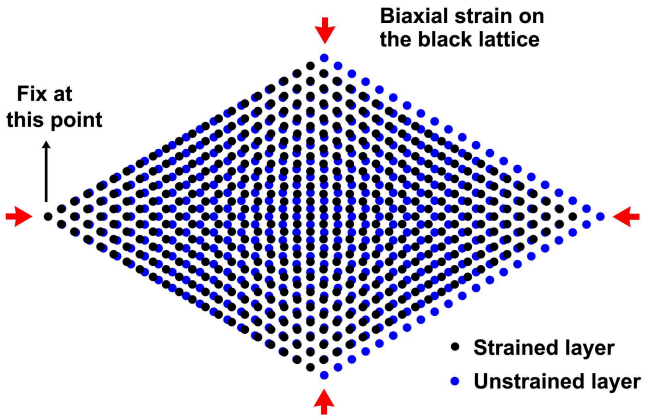

FIG. 3: The two layer MoS_2 system (top view). Only the lattice points are shown. The black points indicate the first layer who has 5 % of biaxial strain. The blue points indicate the second layer which is without the strain. The lattice points of the two layers also coincide at the corners of the strained layer.

the interlayer VDW interaction using the formula:

$$E_{corr} = -\sum_{i}^{N_{at1}} \sum_{j}^{N_{at2}} \frac{C_{6ij}}{r_{ij}^6} f_{dmp}(r_{ij}) \tag{6}$$

Where the index i goes over the atoms in the first layer and j goes over the atoms in the second layer. r_{ij} is the distance between atom i and atom j. C_{6ij} is a coefficient which depends on the types of atom i and atom j:

$$C_{6ij} = \sqrt{C_{6i} C_{6j}} \tag{7}$$

The parameter C_{6i} and C_{6j} are tabulated for each element and are insensitive to the particular chemical situation. The values of C_{6i} for the elements in the first five row of the periodic table are provided in Ref. 9. $f_{dmp}(r_{ij})$ is the damping function whose expression is:

$$f_{dmp}(r_{ij}) = \frac{s_6}{1 + e^{-d(r_{ij}/(R_{0ij})-1)}} \tag{8}$$

s_6 is a global scaling parameter which depends on DFT functionals used. We choose the optimized value for PBE functional ($S_6 = 0.75$) since the structure of MoS_2 is determined by DFT calculations with PBE functional. The coefficient R_{0ij} also depends on the types of atom i and atom j:

$$R_{0ij} = R_{0i} + R_{0j} \tag{9}$$

The values of R_{0i} for the elements in the first five row of the periodic table are also provided in Ref.[9].

To estimate the slip energy, we compute the interlayer VDW energy of the original and slipped systems described above. The energy difference between these two values provides an estimate of the slip energy. Only the interlayer interaction is counted since the change of the energy within the strained layer is captured by the DFT calculation (which does not include the VDW energy). The VDW energy difference calculated from the above method is 5 meV per primitive unit cell of the MoS_2. A similar order of magnitude of slip energy is expected in {001} epitaxy system and the rotated {111} epitaxy system. The computed slip energy will make a negligible contribution to ΔE. Therefore, for simplicity, this term is neglected.

4. II.1.4. Misfit dislocation term

When misfit dislocations are introduced into the epitaxial system, the mismatch strain is partially relieved by the dislocations at the cost of dislocation formation energy. In the {111} or rotated {111} films, we assume that the misfit dislocations do not generate any shearing and rotation component and relieve the same amount of the normal strain in the $\boldsymbol{x}$ and $\boldsymbol{y}$ directions of the growth plane. Meanwhile, it is also assumed that the misfit dislocations are all pure dislocations. At least two sets of the dislocations are needed. In Fig. 4(a), the misfit dislocation geometry (with 2 sets of dislocations) for {111} and rotated {111} orientations is shown. (Note that the Burger's vectors in the rotated {111} are in opposite direction of that in {111}.) The two sets of dislocations must have same spacing within the film in order to exactly cancel the shearing and rotation components. This geometry has the lowest formation energy among the solutions we have considered.

The misfit dislocation geometry in the {001} oriented film is shown Fig. 4(b). In this case, one set of the misfit dislocation relieves the tensile strain in one direction and the other set relieves the compression strain in the perpendicular direction. Similarly, we assume there is no shearing or rotation generated by the misfit dislocations. If the number of sets is restricted to two, this is the lowest energy geometry that satisfies our requirement. In addition, since each set of the dislocations does not introduce a shearing or rotated component, there is no direct constraint between the spacing of the two misfit dislocation sets.

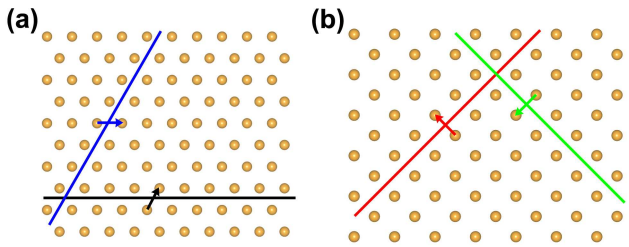

FIG. 4: (color online) (a) The dislocation geometry in Au {111} and rotated {111} orientations. The straight lines indicate the line direction. The arrows with same color give the corresponding Burger's vectors (in rotated {111} the Burger's vectors are in opposite direction). The two sets of the dislocations have same spacing. (b) The dislocation geometry in Au {001} orientation film. There is no direct constraint between the spacing of the two sets.

The formation energy of a misfit dislocation array depends on its spacing, line direction and Burger's vector. The formation energy (per unit cell) of a set of misfit dislocations with a uniform spacing p can be estimated by:

$$E_{dis,i} = \frac{K_i b_i^2}{4\pi p} Log[\frac{4h}{b}] A_f \tag{10}$$

$E_{dis,i}$ stands for the energy contribution from each edge and screw components of the mixed dislocation. E_{dis} is the sum of the contributions from all components (if the dislocation is a pure one, then there is only one component). b_i stands for the projection component of the Burger's vector. K_i is the corresponding anisotropic energy coefficient defined by Hirth *et al*[10], that takes account the elastic anisotropy of the crystalline. h and A_f are the thickness and the unit cell area. In the dislocation geometry of {111} and rotated {111} orientations, each dislocation can be decomposed into three dislocations: a screw dislocation component with a Burger's vector of $\frac{b}{2}$ and a K_i of 16.7 GPa; An edge dislocation component with a Burger's vector of $\frac{b}{2}$ (along $\langle 010 \rangle$ direction of the FCC lattice) and a K_i of 37.9 GPa; Another edge dislocation component with a Burger's vector of $\frac{b}{\sqrt{2}}$ (along $\langle \bar{1}01 \rangle$ direction) and a K_i of 35.5 GPa. The elastic energy of the total dislocation is the sum of the elastic contributions from the three types of dislocations. (For the dislocations in question, there are no cross terms in the elastic energy[10].) In the dislocation geometry of {001} orientation, the dislocations are pure edge dislocations with a K_i of 37.9 GPa (same as one of the edge components in the {111} orientation).

B. II.2. DFT calculation details

DFT based electronic structure total energy calculations are performed using the plane-wave code VASP[11]. The exchange and correlation energy is described by generalized gradient approximation proposed by Perdew, Burke, and Ernzerhof[12]. Electron-ion interactions are treated with projector augmented wave potentials[13]. All calculations are performed using a plane-wave basis with a 350 eV energy cutoff. The precision tag is set to "accurate." The convergence criterion for self-consistent field loop is 1×10^{-8} eV. We use Gaussian smearing method with a smearing width of 0.05. The epitaxial configurations are constructed based on Fig. 1 with the number of Au layers varying from 3 to 30. A 20 Å vacuum slab is added along the direction normal to the growth plane to separate the system from its periodic image. A 14×14×1 Monkhorst-Pack k-point grid is used to sample the Brillioun zone for {111} epitaxy. In {001} epitaxy, a 13×8×1 Monkhorst-Pack k-point grid is used while in the rotated {111}, a 8×8×1 Monkhorst-Pack k-point grid is used. These structures are relaxed until the maximum Hellmann-Feynman force on any atom is below 0.01 eV/Å. Within the density functional theory approach, the change in energy associated with our synthesis path can be written (neglecting the slip energy):

$$\Delta E = E_{tot} - n_{Au} E_{b,Au} - E_{b,MoS_2} \tag{11}$$

with E_{tot} the total energy of the lattice matched slab including one MoS_2 layer and n_{Au} layers of Au (in each unit cell). $E_{b,Au}$ is the energy per layer of bulk unstrained Au and E_{b,MoS_2} is the energy of the monolayer MoS_2. Note that n_{Au} differs between the rotated {111} and the other two structures. Essentially, we use the chemical potential of bulk Au as a reference point for comparing the energies of the rotated {111} structure to the other two.

The parameters that enter the first four contributions to ΔE in linear elasticity theory model are determined either by fitting the results of DFT calculations to the continuum theory or by direct DFT calculations. The DFT calculated lattice structures of bulk Au and monolayer MoS_2 are in good agreement with previous studies. For the bulk Au primitive unit cell, a symmetrized 12×12×12 Monkhorst-Pack k-point grid is used to sample the Brillioun zone. For the primitive cell of monolayer MoS_2, a symmetrized 14×14×1 Monkhorst-Pack k-point grid is used to sample the Brillioun zone. The computed Au lattice constant 4.168 Å, and is in reasonable agreement with experiment result of 4.062 Å and in good agreement

with previous DFT result of 4.154 Å[14]. The in-plane lattice constant of MoS_2 from our DFT calculation is 3.190 Å and the thickness of the monolayer (the separation distance between the top and bottom Sulfur layers) is 3.130 Å. These are also in good agreement with the experimental values of 3.122 Åand 3.116 Å, respectively[15]. The computed elastic constants for these two materials are summarized in Table I.

Our calculated results for gold elastic constants (from GGA PBE) are softer than the experimentally measured values[16]. We also calculated the Au's elastic constants using PAW LDA potential (parameterized by Perdew and Zunger)[17]. The LDA results overestimate the elastic constants of Au, as shown in Table I. We further double checked our epitaxy system calculations (with 3, 21 and 24 layers of Au) using LDA between the two competing orientations, {111} and {001} (for the most cases, the rotated {111} is higher in energy than these two orientations). In the LDA calculations, the {111} epitaxy systems are still more stable than the {001} epitaxy systems, which is consistent with the GGA results. In the Ref. 18, a discussion of the elastic constants of MoS_2 (both measured and predicted) is given. The C_{12} measured experimentally is negative, which contrasts with the positive value computed here and with the DFT-D2 calculations done by Peelaers and van de Walle. Peelaers and van de Walle argued that the C_{12} measurement is indirect, and might be complicated by the lubricating properties of MoS_2. In order to directly compare our results with those in Ref. 18, we follow their convention of calculating the elastic constants for 2D material, in which the thickness of monolayer MoS_2 is chosen to be the half length of the unit cell vector perpendicular to the basal plane in bulk MoS_2 the unit cell contains 2 MoS_2 layers). Our calculated elastic constants are in good agreement with Peelaers and van de Walle's results.

The calculated structures and elastic constants are used for the parameters of our continuum elastic model, *i.e.* the equilibrium volume of the film, the equilibrium area of the substrate/surface/interface and the elastic constants of the film and the top layer substrate. The calculated elastic constants are used for the parameters $C_{f,ijkl}$ and $C_{sub,ijkl}$. The calculated lattice structures are used to determine V_f, A_{sub}, A_s and A_I.

TABLE I: The elastic constants of bulk Au and MoS_2.

	Elastic Constants	GGA [GPa][a]	LDA [GPa]	Experiment [GPa][b]
Au	C_{11}	154	219	192
	C_{12}	136	183	163
	C_{44}	31	41	39
MoS_2	C_{11}	211	237	238 (238)
	C_{12}	53	56	-54 (64)

[a]The GGA (PBE) results are used for the following calculations.

[b]The previous reports of Au elastic constants can be found in Ref[16]. The reported MoS_2 elastic constants is from Ref[18]. The DFT calculated elastic constnats from this reference is in parenthesis.

C. II.3. The minimization of ΔE and fitting processes

1. *II.3.1. ΔE minimization without dislocations*

Before including the misfit dislocations, the equilibrium expression of ΔE (for the "primitive" model) is determined by minimizing ΔE with respect to the strains in the film and the first substrate layer, subjecting to the constraint that the first substrate layer and the film are lattice matched across the interface.

As shown in Fig. 1(a), the lattice mismatch between Au and MoS_2 is about 8% biaxially. Therefore, the Au film has a biaxial tensile strain ($\epsilon_{Au,11}$) in the growth plane and a normal strain component ($\epsilon_{Au,33}$) in the direction perpendicular to the plane. The shear strain is zero. The strain of the interface and surface are the same as the strain of the Au film in the growth plane. The strain for the MoS_2 is a biaxial compressive strain ($\epsilon_{MoS_2,11}$) also with no shear component. With this form of the strain tensor given, the expression of the "primitive" ΔE can be written down based on Eqn. (1) to (5). Furthermore, the value of $\epsilon_{MoS_2,11}$ is related to $\epsilon_{Au,11}$ through the condition of lattice matching at the interface:

$$a_{Au}(1+\epsilon_{Au,11}) = a_{MoS_2}(1+\epsilon_{MoS_2,11}) \tag{12}$$

Once the number of Au layers is given, the only variables in the ΔE's expression are $\epsilon_{Au,11}$ and $\epsilon_{Au,33}$. The ΔE can then be minimized with respect to $\epsilon_{Au,11}$ and $\epsilon_{Au,33}$. Moreover, in this case, only the combined linear term ($f_s + f_I$), the combined quadratic terms ($C_{Sub,1111} +$

$C_{Sub,1122} + C_{I,1111} + C_{I,1122}$) and the combined free interface and surface energies ($\gamma_s + \gamma_I$) enter into the minimized expression for ΔE. (Due to the symmetry of the surface/interface, the linear term can be taken as scalar[19].) Thus these combined terms can be fitted as a whole to the DFT results.

In the case of {001} epitaxy, the lattice mismatch is about 8% in direction **1** and -6% in direction **2**, as shown in Fig. 1(b). In the growth plane, the Au film has a pure tensile strain $\epsilon'_{Au,11}$ in direction **1** and a pure compression strain $\epsilon'_{Au,22}$ in direction **2**. The Au film also has a normal strain component $\epsilon'_{Au,33}$ perpendicular to the growth plane. Similarly, the strain of the interface and surface are same as the strain in the Au film growth plane. In the MoS_2, likewise, it has normal compression strain $\epsilon'_{MoS_2,11}$ in direction **1** and normal tensile strain $\epsilon'_{MoS_2,22}$ in direction **2**. The shear components for both Au and MoS_2 remain zero. There are now two constraint equations relating the strain of Au and MoS_2 in the growth plane:

$$a_{1(Au)}(1 + \epsilon'_{Au,11}) = a_{1(MoS_2)}(1 + \epsilon'_{MoS_2,11}) \tag{13}$$

$$a_{2(Au)}(1 + \epsilon'_{Au,22}) = a_{2(MoS_2)}(1 + \epsilon'_{MoS_2,22}) \tag{14}$$

where $a_{1(Au)}$ and $a_{1(MoS_2)}$ are the lattice parameter in direction 1 while $a_{2(Au)}$ and $a_{2(MoS_2)}$ are the lattice parameter in direction 2 (consistent with Fig. 1(b)). Once the number of Au layers is given, the variables in the total energy expressions are $\epsilon'_{Au,11}$, $\epsilon'_{Au,22}$ and $\epsilon'_{Au,33}$. ΔE can then be minimized with respect to $\epsilon'_{Au,11}$, $\epsilon'_{Au,22}$ and $\epsilon'_{Au,33}$. In this case, we have one combined linear term ($f_s + f_I$), two combined elastic constants ($C_{Sub,1111} + C_{I,1111}$ and $C_{Sub,1122} + C_{I,1122}$) and the combined free surface and interface energies ($\gamma_s + \gamma_I$) entering the minimized ΔE expression. Just as in the case of {111} epitaxy, these parameters are fitted as a whole to the DFT results.

In the case of the rotated {111} epitaxy, the lattice mismatch is about -6% biaxially, as shown in Fig. 1(c) of the main text. In this case, the Au film has a biaxial compression strain ($\epsilon_{Au,11}$) in the growth plane and a normal strain component ($\epsilon_{Au,33}$) in the direction perpendicular to the plane. The shear strain is still zero. The strain of the interface and surface are same as the strain of the Au film in the growth plane. The strain for the MoS_2 is a biaxial tensile strain ($\epsilon_{MoS_2,11}$) also with no shear component. Similarly the value of $\epsilon_{MoS_2,11}$ is related to $\epsilon_{Au,11}$ through the condition of lattice matching at the interface:

$$2a_{Au}(1 + \epsilon_{Au,11}) = \sqrt{3}a_{MoS_2}(1 + \epsilon_{MoS_2,11}) \tag{15}$$

Similar to {111} epitaxy, the "primitive" ΔE can then be minimized with respect to $\epsilon_{Au,11}$ and $\epsilon_{Au,33}$. Also only the combined linear term $(f_s + f_I)$, the combined quadratic terms $(C_{Sub,1111} + C_{Sub,1122} + C_{I,1111} + C_{I,1122})$ and the combined free interface and surface energies $(\gamma_s + \gamma_I)$ enter into the minimized expression for ΔE.

2. *II.3.2. Fitting continuum linear elasticity theory to DFT results*

The results of DFT calculations are used to find optimal parameters for the continuum linear elasticity theory. Briefly, the DFT energy and strain data are fitted to the predictions of the continuum theory. The fitting process chooses the parmeters of the continuum linear elasticity theory to minimize "χ^2":

$$\chi^2 = w \sum_i (\Delta E[i] - \Delta \tilde{E}[i])^2 + (1 - w) \sum_j (\epsilon[j] - \tilde{\epsilon}[j])^2. \tag{16}$$

In the above equation, $\Delta E[i]$ is the DFT calculated excess energy of Au-MoS_2 system with i layer of Au. $\Delta \tilde{E}[i]$ is the minimized excess energy from our model also with i layer of Au. The strain sum term is defined similarly. The indices i and j run over all the DFT data. w is the relative weight parameter for the DFT based energy and strain data. Since the DFT calculated energy is more accurate than the DFT calculated strain, we put more weight (2/3) on the energy terms. The parameters entering the fitted functional forms are displayed in Table II. For {111} epitaxy, the in-plane biaxial strain comes into the strain sum. For {001} epitaxy, both ϵ_{11} and ϵ_{22} come into the strain sum. The expressions for the $\tilde{\epsilon}[j]$ are also obtained through minimizing the ΔE algebraically, and these depend upon the same combinations of the surface/interface terms. The fitted results are summarized in Table II.

3. *II.3.3. ΔE minimization with dislocations included*

Once these parameters are known, we include the misfit dislocations into our linear elasticity theory model and minimized the ΔE respect to both the strains and the spacing of the dislocations. At this stage, the in-plane lattice match condition is also revised with the strain relief effect from the dislocation included. In the {111} orientation, the lattice match

TABLE II: The values of fitting parameters.[a]

	Linear terms	Quadratic terms		Free energy terms
{111} epitaxy	$f_s + f_I$	$C_{Sub,1111} + C_{Sub,1122} + C_{I,1111} + C_{I,1122}$		$\gamma_i + \gamma_s$
	0.167	3.988		0.067
{001} epitaxy	$f_s + f_I$	$C_{Sub,1111} + C_{I,1111}$	$C_{Sub,1122} + C_{I,1122}$	$\gamma_i + \gamma_s$
	-0.541	45.703	45.656	0.099
Rotated {111}	$f_s + f_I$	$C_{Sub,1111} + C_{Sub,1122} + C_{I,1111} + C_{I,1122}$		$\gamma_i + \gamma_s$
	-0.099	-8.770		0.096

[a] All fitting parameters are in unit of [eV/Å^2].

condition can now be written as:

$$\frac{\sqrt{3}b}{2p} = \frac{a_{MoS_2}(1+\eta_{Mo,11}) - a_{Au}}{a_{Au}} - \eta_{Au,11} \tag{17}$$

The amount on the left side is the strain relieved by one set of the misfit dislocations and it makes up the difference between the biaxial strain component in the MoS_2 ($\eta_{Mo,11}$) and the Au film ($\eta_{Au,11}$). The a_{Au} and a_{MoS_2} are the corresponding lattice constants. This equation should be satisfied in both in-plane directions due to symmetry requirement. Since now we introduced one more degree of freedom (dislocation spacing), ΔE is minimized respect to the in-plane strain $\eta_{Au,11}$, out-of-plane normal strain $\eta_{Au,33}$ and dislocation spacing p.

In the rotated {111} orientation, the lattice match condition can now be written as:

$$-\frac{\sqrt{3}b}{2p} = \frac{\sqrt{3}a_{MoS_2}(1+\eta_{Mo,11}) - 2a_{Au}}{2a_{Au}} - \eta_{Au,11} \tag{18}$$

which also should be satisfied for both $\boldsymbol{x}$ and $\boldsymbol{y}$ directions. The minus sign in the left front counts for the fact that the Burger's vector is in the opposite direction of that in {111} orientation. Similar to {111} orientation, ΔE is minimized respect to the in-plane strain $\eta_{Au,11}$, out-of-plane normal strain $\eta_{Au,33}$ and dislocation spacing p.

In the {001} orientation, we need two lattice match equations:

$$\frac{b}{p_1} = \frac{a_{1(MoS2)}(1+\eta_{Mo,11}) - a_{1(Au)}}{a_{1(Au)}} - \eta_{Au,11} \tag{19}$$

$$-\frac{b}{p_2} = \frac{a_{2(MoS2)}(1+\eta_{Mo,22}) - a_{2(Au)}}{a_{2(Au)}} - \eta_{Au,22} \tag{20}$$

In the tensile strain (in terms of Au film) direction, the lattice match condition is Eqn. (19). Eqn. (20) describes the lattice match condition in the compressive strain direction. p_1 and p_2 are the dislocation spacing in the corresponding directions respectively. $\eta_{Au,11}$ and $\eta_{Au,22}$ are the normal tensile and compression strain in the Au film. $\eta_{Mo,11}$ and $\eta_{Mo,22}$ are defined similarly. As mentioned above, there is no direct constraint for the spacings in the two directions. Thus two more degrees of freedom are added to ΔE when the misfit dislocations are included. Now ΔE should be minimized respect to in-plane and out-of-plane strains ($\eta_{Au,11}$, $\eta_{Au,22}$ and $\eta_{Au,33}$) and dislocation spacings (p_1 and p_2). These minimization processes will give us the final expression of ΔE as a function of the Au layer number.

D. III. Results

Fig. 5(a) shows the fitting results for the compliant substrate model without dislcocations, and compares them to the traditional epitaxy model with the surface and interface contributions included, but no misfit dislocations. It is apparent that the elasticity theory based model does an excellent job of describing the DFT calculated excess energies. Meanwhile, within the compliant substrate epitaxial model, beyond 10 Au layers, {111} epitaxy is energetically favored over the other two oriented epitaxy. In contrast to the traditional epitaxy model, the variation of the ΔE with thickness is sublinear in the case of compliant substrate epitaxy. This sublinear behavior originates in the fact that the strain in the film is decreasing as the film thickness increases. As the film gets thicker, it becomes elastically more stiff, and the first layer of the substrate is forced to deform to a greater extent. Eventually, when the Au film is infinitely thick, only the first substrate layer deforms, and the elastic energy saturates at a constant. This trend reduces the tendency towards more complicated growth modes (e.g. Stranski-Krastanov growth). To our knowledge, this reduction in strain energy of the film with increasing film thickness is a unique feature of compliant substrate epitaxy. The fitted strain is shown in Fig. 6. The strain curves are also in reasonable agreement with the DFT data.

Fig. 5(b) shows the results when misfit dislocations are included. As expected, for all three orientations, including misfit dislocations does lower ΔE. For the {111} orientation, the energy reduction is over 0.2 eV per unit cell which further stabilizes this orientation compared to the other two. In addition, the rotated {111} orientation is also shifted to the

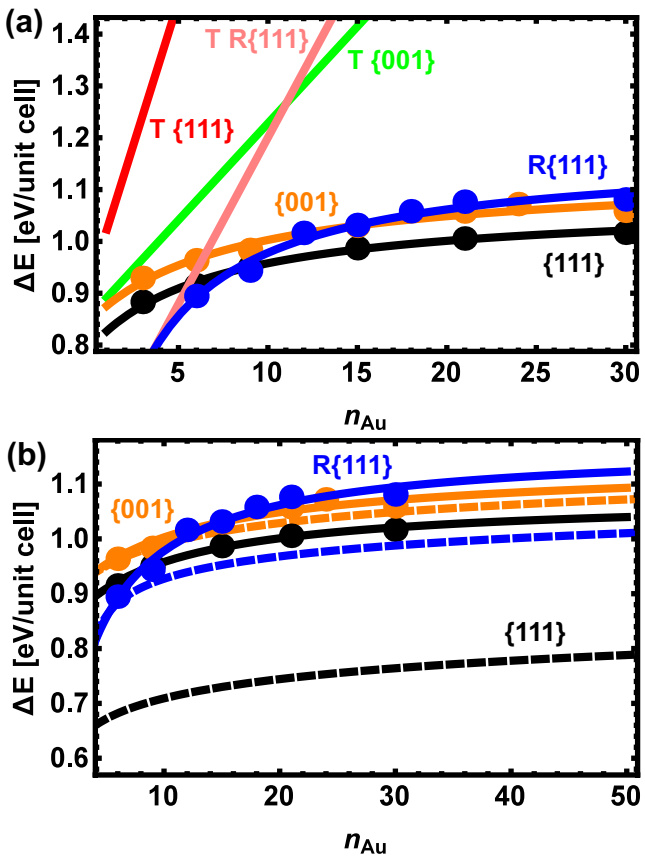

FIG. 5: (a) A comparison between the ΔE of the compliant substrate epitaxy (no misfit dislocations) and that of traditional epitaxy (assuming rigid substrate, labeled with "T" in front). Note that surface and interfacial energies and strain energies are included in the lines labelled with "T". DFT results are shown as dots, and the lines passing through them are the results of the continuum theory fitted to the DFT data. Inclusion of surface/interface effects alone does not stabilize the {111} orientation. (b) When the misfit dislocations are included, the elastic energy for all configurations is reduced as expected. The dashed lines are the results with misfit dislocation and are compared to those without misfit dislocations (solid lines in same color). The {111} orientation is still the lowest energy configuration. Moreover, the curve of the rotated {111} orientation is lowered below that of the {001} orientation by the dislocations.

second lowest place while the {001} orientation receives the least energy reduction. Generally speaking, the configuration with more mismatch strain will receive more energy reduction from introducing misfit dislocation. This is determined by the fact that the formation energy of misfit dislocation scales as $\frac{b}{p}$ and the elastic energy after including the dislocation scales

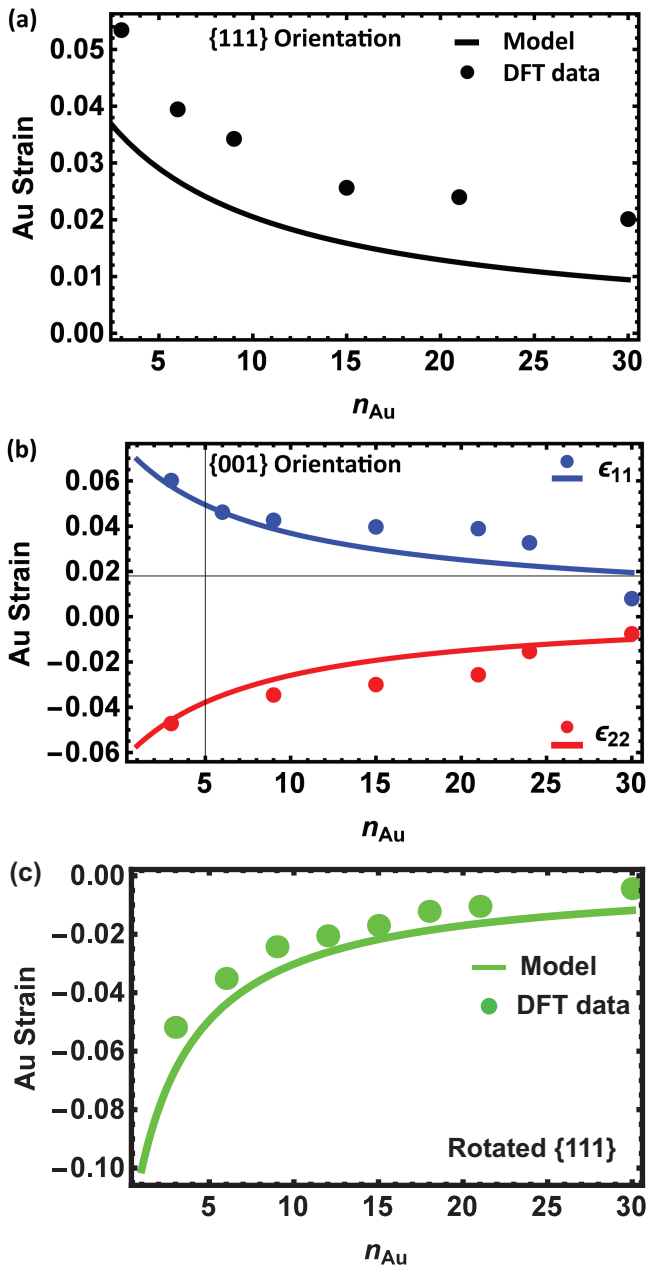

FIG. 6: The fitted Au strain curves and DFT Au strain data as a function of Au layer number for (a) the biaxial tensile strain in {111} orientation. (b) the two in-plane strains in {001} orientation. (c) the biaxial compression strain in rotated {111} orientation.

as $(\epsilon_m - \frac{b}{p})^2$, where ϵ_m is the original strain in the film. For same dislocation formation energy (same $\frac{b}{p}$), a larger mismatch system (larger ϵ_m) will generally receive more energy reduction due to the quadratic behavior of the elastic energy. Therefore, the elastic energy of {111} orientation, which has the largest mismatch (8% biaxial), is reduced the most. The

rotated {111} orientation, with the medium mismatch (-6% biaxial), displays the second largest energy reduction. And the elastic energy of {001} orientation is barely reduced by the dislocations since it has the lowest mismatch (-6% in the one direction and 8% in the other). We note that changing the chemical potential of Au in Eqn. (11), which is equivalent to changing the Au growth condition, could shift the curve of the rotated {111} respect to the other two. However, the predictions here agree with the *in situ* growth experiments of Pashley *et al.*[2], and we expect that in many growth situations the {111} orientation will remain favored.

III. IV. DISCUSSION

The model presented here is not the first proposed that exploits a compliant substrate. As early as 1991, Lo suggested that the quality of some epitaxial films could be improved by employing a compliant substrate[20]. Such a substrate would enable relaxation of the film at the expense of the substrate, but had the potential to increase the quality of the epitaxial film. Lo suggested that such substrates could be produced using standard lithographic methods. Later, Jesser *et al.* proposed that a compliant substrate might be developed by introducing a subsurface twist boundary[21]. Here, it is noted that layered materials with VDW bonding between them form naturally compliant substrates for epitaxial growth. Moreover, the VDW bonding, while enabling lateral slip of the substrate, will resist buckling of the film, and thereby help to improve its quality. Though we have examined Au on MoS_2 in detail, the idea is quite general, and should apply to other systems as well.

The continuum elasticity theory enables investigation of a broader class of models. For example, we can examine a traditional epitaxial system with the introduction of misfit dislocations. The ΔE's of these systems are compared to those of the complete model in Fig. 7. The model without the compliant substrate also predicts that the {111} orientation is favored over the other considered structures. However, upon introducing the compliant substrate, however, the energy of a 30 layer film is reduced approximately 50 meV/unit cell, or approximately 7%. This energy reduction is approximatley 25 times the slip energy per unit cell. We therefore expect the substrate to distort during epitaxy (barring its pinning by defects or some such).

It is also worth noting that the compliant substrate reduces the dislocation density com-

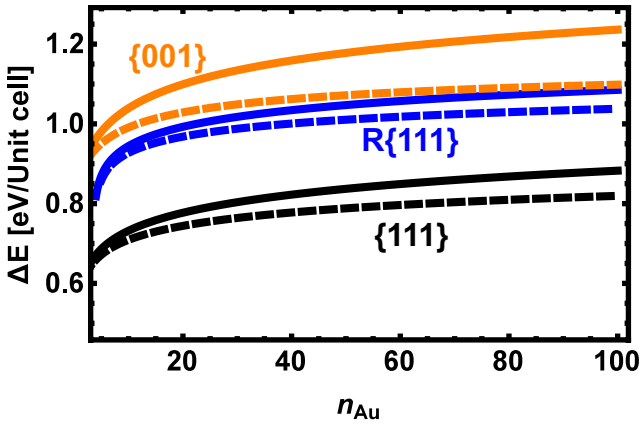

FIG. 7: The ΔE of the epitaxy systems with and without compliant substrate (but all with surface/interface energies and misfit dislocations). The dashed lines are the curves for the systems with compliant substrate and the solid lines are for those without compliant substrate. Enabling compliant substrate does lower the energy. In addition, this reduction increases as the Au film grows.

pared to the traditional epitaxy due to the fact that the substrate partially relieves the mismatch strain. After the minimization of ΔE, the dislocation spacing can also be plotted as a function of the Au layer number, as shown in Fig. 8. In Fig. 8(a), we further compare the equilibrium spacing of the {111} orientation with and without a compliant substrate. It is shown that introducing compliant substrate indeed increases the spacing of the misfit dislocations in all Au thickness range. For example, a 30 layer Au film will have approximately 3.1 nm between misfit dislocations in the traditional substrate model, but will have approximately 4.3 nm between misfit dislocations in the compliant substrate model.

The model also helps to understand the slight rotations observed in the Au islands during the earliest experiments[2]. Based on our misfit dislocation model, this minor rotation can be explained by the imbalance of dislocation spacing (or dislocation number) in the two sets of misfit dislocations in the {111} dislocation geometry (shown in Fig. 4(a)). Based on the dislocation geometry, the displacement field arising from the dislocations are:

$$u_{\boldsymbol{x}} = \frac{\sqrt{3}x - y}{2p_2}b + \frac{y}{2p_1}b \tag{21}$$

$$u_{\boldsymbol{y}} = \frac{\sqrt{3}y}{2p_1}b \tag{22}$$

where $u_{\boldsymbol{x}}$ and $u_{\boldsymbol{y}}$ are the $\boldsymbol{x}$ and $\boldsymbol{y}$ components of the displacement. In an ideal situation,

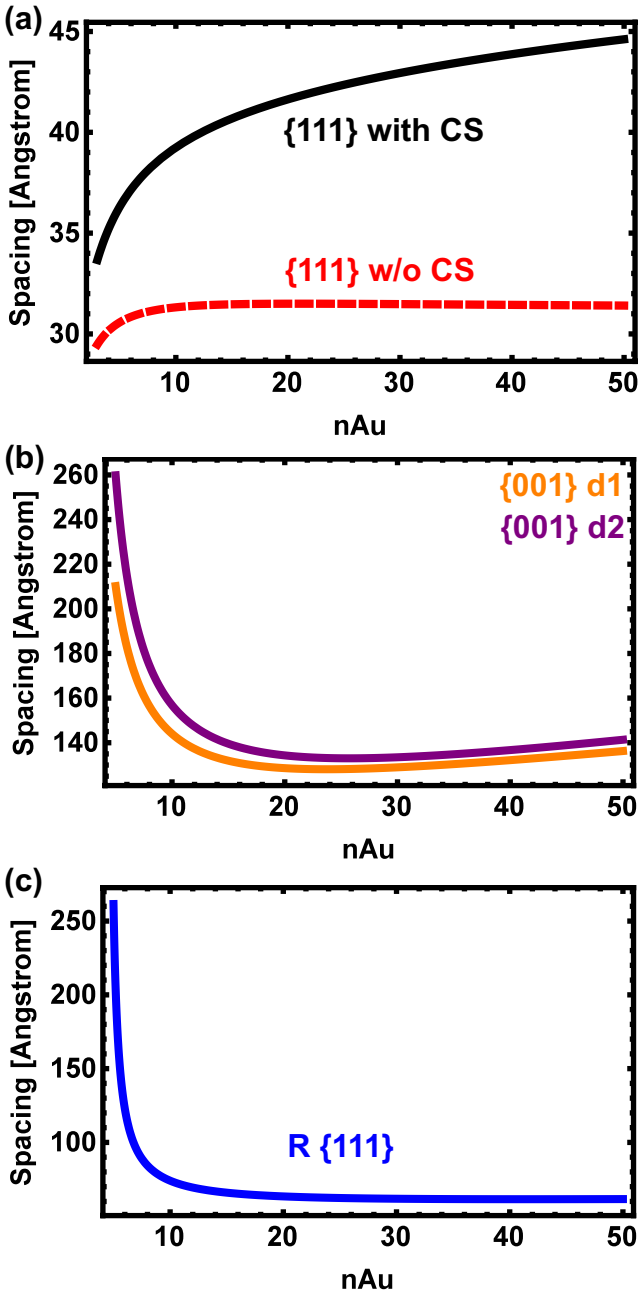

FIG. 8: (a) The equilibrium dislocation spacing in {111} orientation with and without compliant substrate (CS). (b) The equilibrium dislocation spacings for the two sets of the misfit dislocations in {001} orientation in the compliant substrate model. The labels for the in-plane directions are consistent with Fig. 1(b) of the main text. The {001} d1 stands for the spacing of the dislocations that relieve the strain in direction 1 and likewise for {001} d2. (c) The equilibrium dislocation spacing in rotated {111} orientation in the compliant substrate model.

the two sets misfit dislocations will have exactly same spacing ($p_1 = p_2 = p$) and therefore exactly cancel the shearing ($\frac{1}{2}(\frac{\partial u_{\boldsymbol{x}}}{\partial y} + \frac{\partial u_{\boldsymbol{y}}}{\partial x})$) and rotation ($\frac{1}{2}(\frac{\partial u_{\boldsymbol{x}}}{\partial y} - \frac{\partial u_{\boldsymbol{y}}}{\partial x})$) component in the strain field. If there is a small deviation from this condition, say $p_2 = p + \Delta p$, a non-zero rotation of $\frac{b\Delta p}{4p^2}$ radians is generated. Based on the size of the Au islands shown in the TEM figures of Ref.[2] (about 20 nm across) and the spacing-thickness curve in Fig. 8(a) from our model (around 5 nm thickness the spacing is about 4 nm), the estimated rotation calculated from our model is about $\pm 0.26^\circ$, which is in excellent agreement with the experimental observations (0.25°)[2].

A closer look at the fitted free energy terms gives further insight into the properties of the surface/interface. Among three orientations, the {111} orientation has the lowest fitted free energy (see Table II). This is consistent with the fact that the {111} surface is the energetically favorable surface and the fact that the {111} interface has the most direct Au-S bonds (Au directly on top of the S). Moreover, in the {111} and the rotated {111} orientations, they differ only in their Au/MoS_2 interfacial structure (and energy), with the exception of the sign and slight magnitude difference of the strain. When considering the interface, the main difference is the bonding arrangement between the Au and the S atoms. In the {111} orientation, each Au atom of the first deposited layer sits directly above a S atom. In contrast, for the rotated {111} structure, only one in four of the Au atoms sits directly above a S atom, and, presumably, this changes the nature of the bonding across the interface.

This has also been quantitatively reflected in the fitted free energy terms. The free surface/interface energy for the rotated {111} is about 0.03 eV/Å^2 higher than that of the {111} orientation (Table II). Since the surface is same for both orientations, the difference in the free surface/interface energy terms all come from the interface energies. We can further estimate the strength of the Au-S bonding based on above analysis. In a {111} unit cell there is one Au-S bond at the interface. In the same cross-sectional area of the rotated {111} orientation, the number of Au-S bond is fractional (this fraction should be slightly above 0.25, since the Au atoms in the deposited layer which are not directly on the S atoms can still form weak bond with Au). Given that the cross-sectional area of the {111} unit cell is about 10 Å^2, the fractional number difference of Au-S bond gives rise to a 0.3 eV interfacial energy difference. Therefore, the strength of the Au-S bonding in the $Au\text{-}MoS_2$ system is estimated to be on the order of few tenths of an eV to one eV (depending on the

exact number of bonds that form in the rotated {111} structure). The Au-S bond is known to be quite strong from isolated thiols and disulfides[22]. Apparently, in this epitaxial system, the Au-S bond is also relatively strong, and serves to stabilize the observed structure. Given the reference chemical potential used here, the structure and energy of the Au-S interface, underpins the observed energy difference.

This strength appears to not have been anticipated by prior efforts to understand the Au{111}/MoS_2 interface. For example, both refs.[8] and[23] consider the properties of the rotated {111} orientation in their studies of Au/MoS_2 contacts. Both studies conclude that the rotated Au{111}/MoS_2 will pose a high-energy tunneling barrier for electrons. Moreover, Kang *et al.* argue that the rotated Au{111}/MoS_2 produce a "typical" Schottky contact because of the "lack of orbital overlaps"[23]. However, in the theoretically predicted and experimentally observed most stable configuration, there is substantial bonding between the Au and the S atoms, which appears to conflict with the claimed lack of orbital overlap. Perhaps the current understanding of the transport properties of the Au/MoS_2 interface needs to be revisited.

The strong bonding at the Au{111}/MoS_2 interface will also be useful in efforts to manipulate MoS_2. Since this bonding is stronger than the van der Waals bonding of the MoS_2 to itself, we can use the Au{111}/MoS_2 interface to exfoliate and transfer large single layer flakes of MoS_2 to other substrates. Using this idea, we have been able to transfer single layers of MoS_2 that are nearly 0.5 mm in diameter[24]. We note that others have used the Au{111}/MoS_2 interface to create large single layers of MoS_2 and other dichalcogenides bound to a Au surface[25].

We also note that compliant substrate epitaxy may have interesting implications for strain engineering and processing of thin films. Consider the strain field near a small Au island in the early stages of the film growth, in islands less than 4 nm across (so that misfit dislocations are not yet introduced). The MoS_2 under the island will be strained in compression. This will naturally be accommodated by a tensile strain surrounding the island. By engineering the positions of the Au nuclei, one should be able to induce a desired strain pattern into the first layer of the MoS_2 substrate.

IV. V. CONCLUSIONS

In conclusion, the epitaxial growth of Au on MoS_2 is studied using a combination of continuum linear elasticity and density functional theories. It is shown that the compliance of the substrate, in conjunction with the surface/interface energies and the misfit dislocations, stabilizes the {111} growth orientation relative to competing structures despite the large lattice mismatch. Our model is consistent with the experimental observations of the epitaxial growth of Au on MoS_2, and further shows that Au-S bonding is significant. This strong bonding may prove technologically useful in both manipulating and straining MoS_2 monolayers.

Acknowledgments

This work was supported within the Electronic Materials Program at the Lawrence Berkeley National Laboratory by the Director, Office of Science, Office of Basic Energy Sciences, Division of Materials Sciences and Engineering, of the U.S. Department of Energy under Contract No. DE-AC02-05CH11231.

---

[1] B. Radisavljevic, A. Radenovic, J. Brivio, V. Giacometti, and A. Kis, Nature nanotechnology **6**, 147 (2011).

[2] M. H. Jacobs and M. J. Stowell, Philosophical Magazine **11**, 591 (1965).

[3] W. A. Jesser and D. KuhlmannWilsdorf, Journal of Applied Physics **38**, 5128 (1967).

[4] G. Honjo and K. Yagi, Journal of Vacuum Science and Technology **6**, 576 (1969).

[5] D. W. Pashley, M. J. Stowell, M. H. Jacobs, and T. J. Law, Philosophical Magazine **10**, 127 (1964).

[6] M. H. Jacobs, D. W. Pashley, and M. J. Stowell, Philosophical Magazine **13**, 129 (1966).

[7] W. A. Jesser and D. Kuhlmann-Wilsdorf, Phys. Stat. Sol. **19**, 95 (1967).

[8] I. Popov, G. Seifert, and D. Tománek, Phys. Rev. Lett. **108**, 156802 (2012), URL `http://link.aps.org/doi/10.1103/PhysRevLett.108.156802`.

[9] S. Grimme, Journal of Computational Chemistry **27**, 1787 (2006), ISSN 1096-987X, URL `http://dx.doi.org/10.1002/jcc.20495`.

[10] J. P. Hirth and J. Lothe, *Theory of Dislocations* (Krieger Publishing Company, Florida, USA, 1991).

[11] G. Kresse and J. Hafner, Phys. Rev. B **47**, 558 (1993), URL http://link.aps.org/doi/10.1103/PhysRevB.47.558.

[12] J. P. Perdew, K. Burke, and M. Ernzerhof, Phys. Rev. Lett. **77**, 3865 (1996), URL http://link.aps.org/doi/10.1103/PhysRevLett.77.3865.

[13] G. Kresse and D. Joubert, Phys. Rev. B **59**, 1758 (1999), URL http://link.aps.org/doi/10.1103/PhysRevB.59.1758.

[14] P. Haas, F. Tran, and P. Blaha, Phys. Rev. B **79**, 085104 (2009), URL http://link.aps.org/doi/10.1103/PhysRevB.79.085104.

[15] E. S. Kadantsev and P. Hawrylak, Solid State Communications **152**, 909 (2012), ISSN 0038-1098, URL http://www.sciencedirect.com/science/article/pii/S0038109812000889.

[16] J. R. Neighbours and G. A. Alers, Phys. Rev. **111**, 707 (1958), URL http://link.aps.org/doi/10.1103/PhysRev.111.707.

[17] J. P. Perdew and A. Zunger, Phys. Rev. B **23**, 5048 (1981), URL http://link.aps.org/doi/10.1103/PhysRevB.23.5048.

[18] H. Peelaers and C. G. Van de Walle, The Journal of Physical Chemistry C **118**, 12073 (2014), http://dx.doi.org/10.1021/jp503683h, URL http://dx.doi.org/10.1021/jp503683h.

[19] R. C. Cammarata and K. Sieradzki, Annual Review of Materials Science **24**, 215 (1994), URL http://dx.doi.org/10.1146/annurev.ms.24.080194.001243.

[20] Y. H. Lo, Applied Physics Letters **59**, 2311 (1991).

[21] W. A. Jesser, J. H. van der Merwe, and P. M. Stoop, Journal of Applied Physics **85**, 2129 (1999).

[22] H. Gröbeck, A. Curioni, and W. Andreoni, Journal of the American Chemical Society **122**, 3839 (2000).

[23] J. Kang, W. Liu, D. Sarkar, D. Jena, and K. Banerjee, Physical Review X **4**, 031005 (2014).

[24] S. B. Desai, S. R. Mahvapathy, M. Amani, D. Kiriya, Y. Zhou, J. A. III, D. C. Chrzan, and A. Javey, we plan to detail the exfoliation process in a future publication.

[25] G. Z. Magda, J. Peto, G. Dobrik, C. Hwang, L. P. Biro, and L. Tapaszto, Scientific Reports (2015).